11-2023

Applications of Femtosecond Laser-Processed and Nanoneedle-Synthesized Surfaces to Enhance Pool Boiling Heat Transfer

Peter Efosa Ohenhen
University of Nebraska-Lincoln, pohenhen2@huskers.unl.edu

APPLICATIONS OF FEMTOSECOND LASER-PROCESSED AND NANONEEDLE-SYNTHESIZED SURFACES TO ENHANCE POOL BOILING HEAT TRANSFER

By

Peter Efosa Ohenhen

A THESIS

Presented to the Faculty of

The Graduate College at the University of Nebraska

In Partial Fulfillment of Requirements

For the Degree of Master of Science

Major: Mechanical Engineering & Applied Mechanics

Under the Supervision of Professor George Gogos

Lincoln, Nebraska

November, 2023

APPLICATIONS OF FEMTOSECOND LASER-PROCESSED AND NANONEEDLE-SYNTHESIZED SURFACES TO ENHANCE POOL BOILING HEAT TRANSFER

Peter Efosa Ohenhen, M.S.

University of Nebraska, 2023

Advisor: George Gogos

In the present work, the integration of femtosecond laser surface processing (FLSP) with copper hydroxide on hybrid surfaces was examined. The goal was to determine the impact on pool boiling enhancement. The samples for the investigation were fabricated by first functionalizing with FLSP, and the process was then followed by citric acid cleaning (CAC) to eliminate the oxides generated on the copper surface during the FLSP process. After the citric acid cleaning, the samples were immersed in ethanol and subjected to an ultrasonic bath for 25 minutes. This step was performed to eliminate any residual citric acid and loose particles. Copper hydroxide nanoneedles (NN) were then synthesized on the FLSP surface. Lastly, some selected samples were heat-treated (HT) at 200^{o}C for 30 minutes to ensure the nanoneedles were secured in place even after several pool boiling runs. The study showed that heat-treated nanoneedle surfaces offer enhanced pool boiling performance compared to untreated ones, and the results are consistent and repeatable. Sample E (FLSP+CAC+NN+HT) exhibited a critical Heat Flux (CHF) of 116.1 W/cm^2 and a heat transfer coefficient (HTC) of 50.5 kW/m^2-K which outperformed sample C (FLSP+CAC+NN) that exhibited a CHF of 100 W/cm^2 at an HTC of 45.2 kW/m^2-K. It was observed that the inclusion of nanoneedles resulted in diminished performance when compared to a polished copper surface. The decline was attributed to the decomposition of

copper hydroxide into copper oxide, consequently introducing insulating material to the surface. Boiling inversion was observed on all tested nanoneedle surfaces.

To my wife, Stephanie.

And to my son Asher for their continuous support and patience

ACKNOWLEDGEMENTS

My appreciation goes to God for continuous grace and guidance. I would also like to say a big thank you to my advisor, Dr. George Gogos for the opportunity and the learning process. Your guidance, advice, and support are greatly appreciated. I am more enlightened on how to approach problems and proffer solutions; my communication skills have also increased greatly. I have learned a lot from you.

I would also like to thank my committee members Dr. Craig Zuhlke, and Dr. Jeffrey Shield for the support offered during my program.

A very big thank you to Justin, Logan, Josh, Henry, Graham, Suchit, Daniel, Sunil, and Chase for always having my back. You all have been a great source of strength and push, always ready to help through challenges.

I would also like to thank Dr. Zhang for the opportunity to work with him and for all the useful advice received.

Many thanks to the family of Mr. and Mrs. Edward Okpa and Pastor and Mrs. Niyi Fanimo for the constant support, and friends that I can call brothers, I cherish the moments. Abraham, Emmanuel Ani, Udochukwu, Viyon, Uche, Prince Mensah, and Oghenetega thank you all.

Work hard and stay humble.

TABLE OF CONTENTS

LIST OF FIGURES

LIST OF TABLES

LIST OF EQUATIONS

CHAPTER 1

INTRODUCTION

Due to the simplicity and the efficacy of dissipating heat energy, cooling via phase transition heat transfer is an efficient application in processes that require the removal of high-density heat [1]. Heat dissipation is a problem that affects many industries, including electronics, transportation, and energy. Due to the growing urge to build smaller and more powerful devices, excessive heat emission frequently becomes the primary design limitation. [2, 3]

During pool boiling, the dissipation of heat from a sample is aided by different mechanisms. These could include natural convection from the heated sample to the surrounding liquid. It also comprises of the overall convection from bubble formation and separation, and latent energy transferred by the working fluid to the bubbles generated at the sample's surface [1]. It is essential to improve these heat transfer mechanisms due to the development of contemporary, high-performance systems that contain electronic components that emit high amounts of heat [1, 4] . The incorporation of boiling mechanisms into cooling systems which uses up the latent heat of vaporization generated during boiling, is one frequent method for dealing with this problem [1]. This enhancement would promote bubble nucleation at low superheats and improve both the heat transfer coefficient (HTC) and the critical heat flux (CHF). Also, the devices can function at lower temperatures and have longer lifespans [2]. The CHF and the HTC are two important variables that can be raised to improve heat transmission during the boiling process.

Several boiling heat transfer improvement methods have been demonstrated in the literature. These methods such as microscale, nanoscale, multiscale, hybrid-wettability, and macroscale have either tried to alter the characteristics of the working fluids or enhance the material surface

morphology [4]. The modification can occur by laser processing of the sample surface, vibration of the heating surface or the addition of substances such as nanoparticles in fluid or nano-coating the materials [5]. Femtosecond laser processing uses ultra-short laser pulses to create micro- and nanostructures on a range of materials while nanoneedle synthesis focuses on creating protrusions on a surface at the nanoscale. These techniques offer precise control over surface shape and may greatly increase heat transfer effectively [6].

1.1 Related Literature Reviews

1.1.1 Pool Boiling with Polished and Processed Copper Surface

Enhanced boiling has emerged as a viable solution to address the challenges brought about by the rapid advancement of technology spanning across various industries [7]. This method becomes significant in the utilization of non-traditional energy sources with low heat flux, and it aligns with the crucial goal of preserving both material and energy resources [8]. In recent decades, various methods for improving heat transfer during boiling have been experimented. Several researchers have undertaken thorough assessments of these methods organizing them into two overarching categories: active and passive techniques [9] [10]. Comparatively, passive techniques have garnered attention for their ability to enhance the boiling heat transfer rate significantly. One noteworthy advantage of passive techniques is the simplicity and cost-effectiveness in fabrication, as they do not rely on external power sources. A pivotal aspect in the quest to optimize the boiling heat transfer efficiency is the creation of specialized boiling surfaces, particularly those featuring micro/nanostructures. The surface properties often include the material composition, geometric configuration, orientation, wettability, surface roughness, and surface characteristics.

Consequently, these attributes have been the focus of extensive study and scrutiny in the pursuit of enhancing boiling [10].

The practice of preparing nanofluids and depositing them onto metallic surfaces for the purpose of augmenting heat transfer performance has been well-established. In this context, using de-ionized water, the impact of a layer coated in zirconia nanoparticles was examined by Gajghate et al [11]. A sequence of assessments including turbidity, viscosity, and stability tests were conducted to affirm the effective dispersion of nanoparticles within the medium. The zirconia nanofluid made synthetically was subsequently deposited onto three copper samples at varying concentrations, employing the nanofluid boiling nanoparticle technique [11].

The outcomes derived from the non-coated copper sample exhibited a close alignment with the Rohsenow correlation, underscoring the reliability and steadfastness of the findings [11]. The experimental results unveiled a remarkable 31.52 % improvement in HTC for samples featuring a surface roughness of 227 nm and coating thickness of 200 nm as opposed to polished copper [11]. Furthermore, the behavior of the bubble within these samples exhibited the maximum velocity and the minimum bubble diameter when subjected to a heat flux of 785 kW/m^2. Consequently, this investigation conclusively demonstrated that the properties of copper substrates coated with zirconia significantly enhanced the pool boiling HTC, particularly at the highest surface roughness and coating thickness [11].

The impact of surface roughness on heat transmission efficiency during pool boiling for both water and FC-77 was investigated by Jones et al [12]. The Samples with different surface roughness were compared to a polished surface as baseline. It was observed that the heat transfer coefficient for FC-77 improved linearly as surface roughness increased, but for water improvement stopped at 1.08 μm. The boiling characteristics of permeable metal coatings were studied experimentally

by Bergles, and Chyu [13]. The study showed an increase in HTC of about 250 % for water and 800 % for R-113. Unlike the aging effects associated with textured surfaces, the permeable coatings offered predictable and repeatable performance as proven by Borzenko, and Malyshenko [14].

Numerous studies have also explored the impact of particle permeability, thickness, and dimension on the boiling performance of sintered materials considering various parametric effects. Li, and Peterson [15] examined the impact of sintered copper wire screens with different thicknesses, porosities, and mesh sizes on the efficiency of boiling. A rise in HTC was observed for small heat fluxes as the thickness of the coating increased, but at high heat fluxes an ideal layer thickness was discovered that resulted in the highest HTC. An increase in the thermal conductivity of permeable coatings resulted in a corresponding increase in CHF. Additionally, a smaller pore size produced a better HTC and a lower boiling incipience superheat [15].

Surface modification techniques improve the removal of large heat fluxes at low superheat. Research has been conducted to investigate the pool boiling behavior of aluminized copper surface using DI water [16]. This process of aluminizing involved immersing the copper specimen in a powder mixture containing Al_2O_3, Al, and NH4Cl, followed by heating treatment. A notable enhancement was observed, with the CHF registering an approximate increase of 37 % on the aluminized surface when compared to the plain copper surface with a CHF of 89.6 W/cm^2. However, the alterations in the HTC were found to be negligible [16]. Therefore, this coating method offers a means to alleviate certain unfavorable characteristics associated with copper, such as oxidation and the relatively low CHF [16].

1.1.2 Heat Transfer Behavior of Plain and Laser-Processed Copper Surfaces

Može et al [17] generated a self-organized micro/nanostructured surface on copper substrates through the utilization of nanosecond fiber laser of wavelength 1060 nm. This study delved into the alterations that took place on copper samples, scrutinized through SEM imaging, XPS, AES, and EDS analyses. The juxtaposition of parallel laser scanning lines induced the formation of multiscale microcavities on the copper specimens with diameters ranging from 0.35 to 5.6 μm. This is attributed to the overlapping of resolidified material on the specimen. To secure the assured formation of microcavities and attain a broad spectrum of radii, a specific blend of laser beam parameters and texturing pattern geometry was employed [17].

The results of this laser-texturing project included a noticeable improvement in the copper surfaces' ability to transport heat during pool boiling tests. Repeated formation of a vapor film and the attainment of temperatures of up to 320 °C during the tests resulted in changes in the surface chemistry and nanomorphology At temperatures as high as 320 °C and the cyclic appearance of a vapor coating led to changes in the surface nanomorphology and chemistry. The laser-processed surfaces showed a CHF improvement of about 90 % and an HTC improvement of over 115 % in comparison to the polished copper sample with a CHF of 83.5 W/cm^2 [17]. A 20% reduction in CHF was observed during subsequent runs, this was as a result of the chemical and morphological changes after the first pool boiling experiment. The wettability of the surfaces changed with surfaces transitioning from hydrophilic to hydrophobic after boiling [17]. In a preceding investigation, the impact of layers of oxide on the heat transfer characteristics of copper surfaces adorned with micro/nanostructures, utilizing a femtosecond laser surface processing (FLSP) was studied by Kruse et al [18]. The objective of this research was to gain a comprehensive understanding of how alterations in oxide layer thickness and the laser fluence parameter

influenced the HTC and CHF of the copper surfaces. Furthermore, it aimed to unveil the intricate interplay between oxide layer thickness and microstructure height and to draw comparisons between the heat transfer performance of copper surfaces including and excluding the oxide layer [18]. The highest CHF obtained for FLSP copper samples was 143.1 W/cm^2 which showed a reduction in CHF when compared to polished copper reference surface that was 169 W/cm^2. However, the outcomes of this research revealed a consistent reduction in both CHF and HTC for FLSP-treated copper surfaces. This decline in heat transfer efficiency was caused by a layer of oxide enveloping the microstructures, functioning as an insulating barrier due to its limited thermal conductivity [18]. It was observed that as the thickness of the layer of oxide increased the permeability also increased with the pores being replete with air. This resulted in an increase in the heat resistance property of the surface thereby reducing the heat transfer performance [18].

Furthermore, heat transfer behavior of copper was studied by Anderson et al [19] after being processed using a picosecond laser pulse technique. It was discovered that the presence of oxides on the treated copper's surface had a detrimental impact on its ability to transport heat. At heat fluxes greater than 90 W/cm^2, the polished reference sample outperformed the oxide-free surfaces with low pulse count in terms of thermal transfer capabilities. The polished reference sample attained an optimal HTC of 54,300 W/m^2K at a CHF of 146 W/cm^2 and a wall superheat of 26.9 ^oC. At a pulse frequency of 1147, the highest CHF obtained with as-processed copper samples was 111 W/cm^2. The citric acid cleaned laser processed surfaces yielded a maximum HTC of 57,800 W/m^2K and was obtained at a CHF of 105 W/cm^2 at a pulse frequency of 719 [19]. It was reported that the oxides could be effectively removed by citric acid treatment. However, it was discovered that doing so decreased the thermal qualities of surfaces with higher pulse count. This action left

behind voids, or onion-like subsurface layers which were undesirable for heat transmission [19]. Figure 1 below depicts boiling curves for both high and low femtosecond laser fluences.

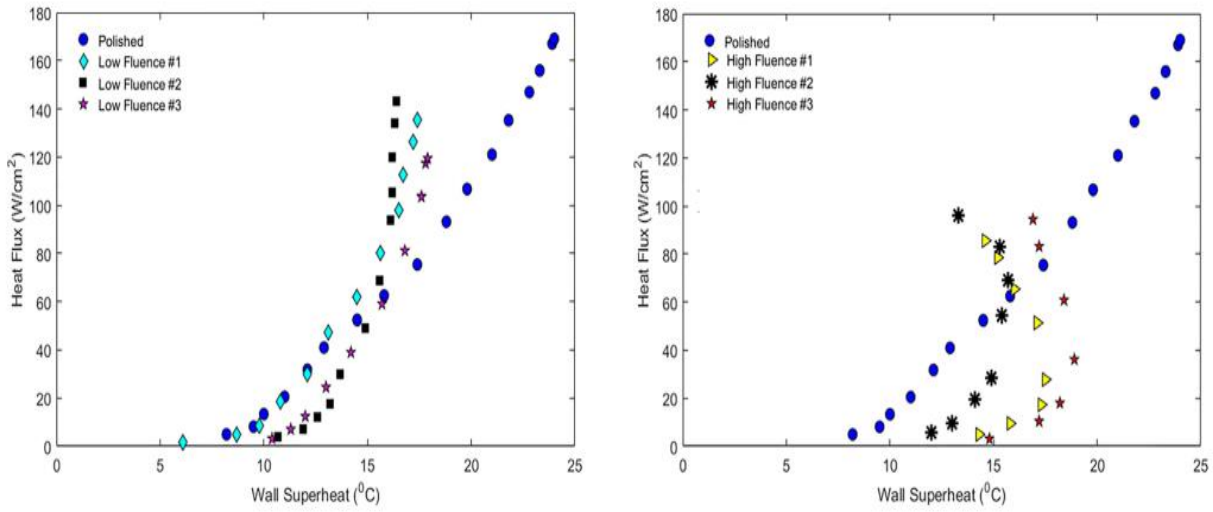

Figure 1. Pool boiling curves for the Low and High Femtosecond Laser fluences [18].

Copper surfaces processed with femtosecond and picosecond lasers showed decreased CHF and HTC in comparison to plain copper samples as drawn from these studies [18, 19]. Mani et al [20] investigated the use of laser-textured copper-grooved surfaces and when compared to plain copper, the laser-processed surfaces with grooves displayed improved surface characterization. At a wall superheated temperature of 28.9 °C, the CHF for the untreated copper surface was 111.3 W/cm^2. Both CHF and HTCs rose with increments in the depth of grooves for the samples processed with laser. The sample with the maximum depth of 100 μm gave the maximum CHF and HTC of 226.3 W/cm^2 and 9.8 W/cm^{2}K respectively [20].

1.1.3 Heat Transfer Behavior of Copper surfaces Processed with other Techniques.

Das et al [21] used a technique called electron beam physical vapor deposition (EBPVD) to create well-organized nanoparticle-coated microstructures on copper surfaces. After three experimental runs, it was observed that the HTC of nanoparticle-coated surfaces remained almost unchanged.

The highest Heat Flux attained was greater than 138 W/cm^2, CHF was not attained [21]. Figure 2 below is a boiling curve that depicts the change in heat flux with superheat for various fabricated samples.

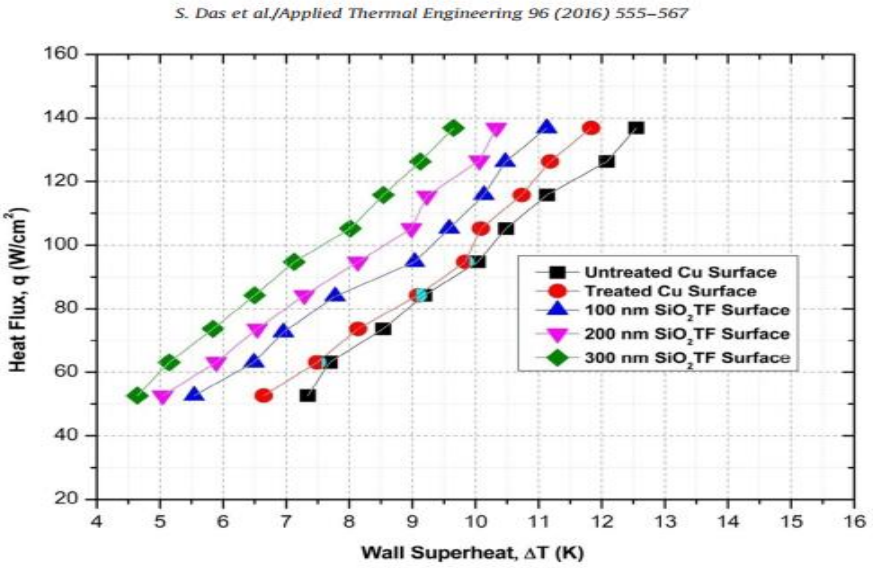

Figure 2. The change in heat flux against superheat for five heating surfaces [21].

Shi et al. [22] studied the impact of utilizing copper nanowire arrays. These nanowires were fabricated onto a plain copper substrate through electroplating, using a porous alumina membrane template that is readily accessible on the market. The highest CHF attained was 230 W/cm^2 for the nanowire sample at a lower superheat and a nanowire length of 30 μm while 145 W/cm^2 was obtained for the plain copper [22]. The Boiling curves in Figure 3 below illustrate the outcome of the boiling experiment with a plain copper surface and nanowire.

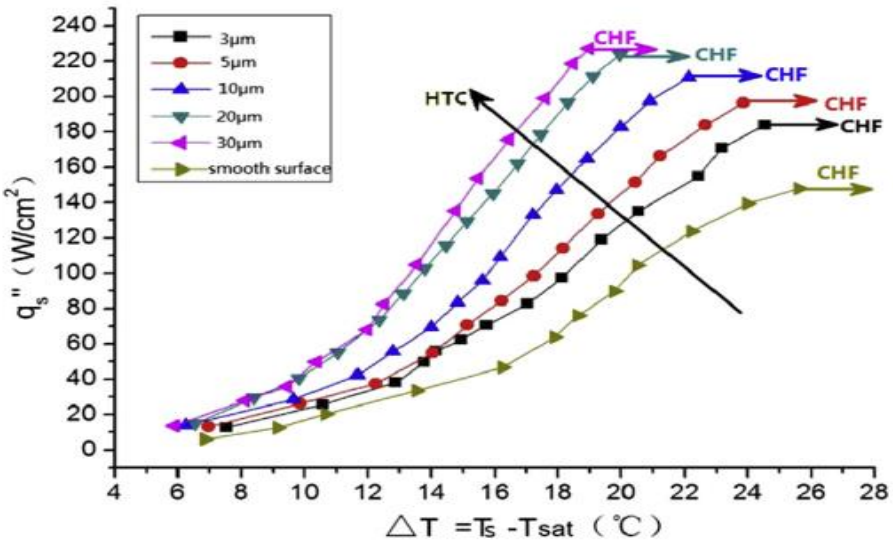

Figure 3. Boiling curve comparing samples with nanowire arrays and plain copper surface [22].

Yang et al [23] examined the heat transfer from boiling pools using copper foams, due to its large porosity . The samples for this test were fabricated by welding pieces of copper foams with varying thicknesses onto a polished copper substrate. The results from this investigation showed that small ppi values (pores per inch) required thick foam covers, while large ppi values typically needed thin covers to improve the thermal properties. It was possible to attain a CHF of 165 W/cm^2 for the unprocessed copper sample. At the same superheat, small ppi resulted in a reduction in the amount of heat released with a corresponding increase in temperature of the working fluid [23]. Arvind Jaikumar and Satish Kandlikar [24] selectively coated various areas of a heat transfer surface, leading to the creation of distinct liquid-vapor channels. Porous coatings were deposited on copper substrate on an open microchannel. A CHF enhancement of 144.5 % was achieved for the processed surface at a lower superheat of 7.5 ^{o}C when compared to the plain copper with a CHF of 1280 kW/m^2 at a superheat of 19.5 ^{o}C. These results were obtained for the sample which was sintered throughout the entire microchannel surface [24].

Through a multistep electrodeposition technique, a covering of copper and graphene nanoplatelets (GNP) was created, and these surfaces were examined during pool boiling [25]. A variety of hierarchical porous coatings were produced, which were superhydrophilic with extremely high wicking rates. The sample with 2% GNP/Cu (wt./vol.) showed 130 % improvement in CHF at a wall superheat of 14.1 ^{o}C in contrast to the polished copper sample which had a CHF of 125 W/cm^2 [25]. Wang et al [26] experimentally examined the combined influence of surface wettability and microporous coating on copper surfaces using distilled water as the working fluid. The samples were produced by utilizing a sintering method in which copper particles were applied over a copper surface and sintered at high temperature in a vacuum furnace. A CHF of 110 W/cm^2 was attained for pure copper surface. The highest CHF of 235 W/cm^2 was achieved for Cu- HTCMC+CuO which corresponds to 114 % enhancement over plain copper surface [26].

Rishi et al [27] utilized a process of multistep electrodeposition to produce porous copper surface coatings. The purpose of the multi-step electrodeposition was to strengthen the bond between the coatings and the copper substrate. A CHF of 125 W/cm^2 and HTC of 52.4 kW/m^2 °C were acquired for the plain copper surface. A 55 % CHF and 92.7 % HTC enhancement over a plain surface at a very low wall superheat of 18.8 °C were obtained for the six-step electrodeposited sample [27]. MacNamara et al [28] experimentally used cold spray fabrication method to deposit thin copper-diamond hybrid layers, forming copper-diamond textured surfaces. These surfaces were utilized to carry out pool boiling experiment with DI water. A CHF of 117.8 W/cm^2 was attained for plain copper reference surface while a CHF of 156.4 W/cm^2 was obtained for the processed surface. The difference in CHF when compared between the plain and the processed copper surface was about 32.8 % enhancement. Boiling inversion was observed at a CHF of 110 W/cm^2 for the processed surface [28].

Jaikumar et al [29] investigated the combination of copper and Graphene Oxide (GO) coatings by utilizing two coating methods which are electrodeposition and screen printing. The experimental results with distilled water at atmospheric pressure showed a CHF and HTC, of 128 W/cm^2 and 65 kW/m^{2o}C for plain copper reference surface. An enhancement of 71.9 % and 138.5 % were obtained for CHF and HTC respectively for the sample with 2.5 % Graphene Oxide, when compared to pure copper surface. The outcome also gave a 43 % reduction in wall superheat [29]. The impact of surface orientation on pool boiling performance for plain and tailored surfaces using different coolants was studied by Munonyedi et al [30]. Regardless of the working fluid type, surface orientation continues to have an impact on CHF and HTC during nucleate pool boiling [30]. Table 1 Below is a summary of HTC obtained with plain and processed copper surfaces from the reviewed literature.

*Table 1**:** Summary of Literature Trends with Polished Copper and Processed Copper Surfaces*

Year	**CHF (W/cm2) Plain Copper Surface**	**CHF (W/cm2) Processed Sample**	**Reference**
2019	169	143.1	[18]
2015	89.6	122.7	[16]
2019	83.5	158	[17]
2016	> 138 (CHF not reached)	-	[21]
2015	~ 145	~ 230	[22]
2010	165	-	[23]
2015	128	313	[24]
2020	111.3	226.3	[20]
2022	146	111	[19]
2019	125	286	[25]

2022	110	235	[26]
2018	125	192	[27]
2019	117.8	156.4	[28]
2017	128	220	[29]

The analysis drawn from related literatures showed that the CHF values for plain copper surfaces range from 83.5 W/cm^2 to 169 W/cm^2, while as high as 313 W/cm^2 has been obtained with processed surfaces. Surface modification of copper using FLSP has shown a limitation. this involves the presence of oxides which often result in a reduction of the heat transfer performance [18, 19]. Costa-Greger et al [31] after citric acid cleaning to reduce these oxides from copper FLSP surfaces, synthesized copper hydroxide nanoneedles on the FLSP surface to enhance the pool boiling heat transfer. These needles were detached from the surface during pool boiling process which has a negative impact on the heat transfer performance.

1.2 Objectives of Current Study

1. Investigate the factors leading to the detachment of copper hydroxide nanoneedles from the copper surface during pool boiling.
2. Determine precisely when in the pool boiling process the nanoneedles become separated from the copper surface.
3. Develop methods to firmly anchor copper hydroxide nanoneedles onto the copper surface, ensuring their retention even after the pool boiling process.
4. Enhance the heat transfer capabilities of the copper surface following pool boiling while simultaneously maintaining the attachment of copper hydroxide nanoneedles.

CHAPTER 2

FEMTOSECOND LASER SURFACE PROCESSING

Introduction

Femtosecond laser technology has become a revolution in the field of surface processing in the past few years. Femtosecond lasers are distinguished by an extremely short pulse durations in the femtosecond range (1 femtosecond equals 10^{-15} seconds). It has spurred an explosion of creativity in the manipulation, alteration, and creation of materials at scales previously considered to be unreachable.

Femtosecond laser technology offers some exceptional features such as the capacity to deliver ultrafast, ultraprecise, and non-thermal laser-matter interactions. The lasers interact with materials far more quickly than ordinary lasers, leaving almost no time for heat to dissipate. As a result of the ultrafast process minimized collateral damage, there are fewer heat-affected zones and less material deterioration. Femtosecond laser technology has a wide range of applications in different sectors; these include optics, electronics, biology, materials science, and manufacturing among others.

2.1 Femtosecond Laser Technology

Numerous academic investigations and real-world applications serve as examples of the femtosecond laser technology's promise for surface treatments. For instance, femtosecond laser-induced periodic surface structures (LIPSS) in the field of photonics have been used to create photonic devices with specialized optical properties [32]. Due to the accuracy and limited invasiveness, femtosecond laser-assisted procedures have become more popular in biomedicine [33]. Additionally, high-precision microstructures in semiconductors for improved electronics have been made possible by femtosecond laser ablation [34].

To investigate the various characteristics, uses, difficulties, and prospects of this revolutionary technology in surface processing, Vorobyev and Guo [35] examined the applications of direct

femtosecond laser surface nano/micro structuring. To stand out among traditional laser ablation techniques, direct femtosecond laser surface processing has garnered attention for its versatility, ease of use, and precise control when generating diverse nano/microstructures. This method has become a leading approach for fabricating surface structures at the nano- and micro-scales on both metals and semiconductors due to its applicability across a wide range of uses. Consequently, this process has led to the production of highly light-absorbent materials, commonly referred to as 'black metals' and 'black silicon'. Furthermore, structural coloring techniques have been applied to metals, resulting in the creation of colors beyond black. In addition, through direct femtosecond laser processing, new materials exhibiting wetting properties spanning from superhydrophilic to superhydrophobic have been developed [35].

FLSP has also been used for the fabrication of superhydrophobic surfaces capable of sustaining an air layer (plastron) between the surface and the encompassing liquid, even when fully immersed. The material used included a grade 2 titanium and 304 stainless steels [36]. It was established that the precise degree of surface micro- and nano-roughness can be modified through the manipulation of various FLSP parameters. This alteration shows a significant dependence on the plastron's duration when exposed to deionized water or simulated gastric acid. In the study, a 304 stainless steel specimen, when immersed in distilled water, exhibited a plastron that persisted for the entire 41-day duration, marking the longest recorded plastron lifetime. This study showcased precise manipulation of pulse fluence and pulse count to create three distinct categories of micron/nano-surface structuring on titanium [36]. A variety of surfaces can be functionalized using femtosecond laser surface processing, incorporating specific attributes such as enhanced broadband optical absorption.

The subjection of amorphous and polycrystalline Ni60Nb40 samples to FLSP with each characterized by different grain sizes, exhibited the formation of two discrete categories of surface structures. These categories are associated with below-surface growth (BSG) and above-surface growth (ASG) mounds [37]. The characterization of the surface showed that the mounds of BSG type, generated on all three substrates under identical laser conditions, exhibited analogous surface characteristics. The mounds' microstructures were unaltered by the laser treatment relative to the substrate, indicating that preferential valley ablation was primarily responsible for the development. The fabrication on polycrystalline Ni60Nb40 surfaces with grain sizes of 100 nm and 2 μ m, the ASG mounds displayed a comparable morphology. However, a noticeable difference was observed when similar ASG mounds were formed on an amorphous Ni60Nb40 substrate. The increased size of ASG mounds on amorphous Ni60Nb40 substrates resulted from the substrate's lower thermal diffusivity [37].

Ley et al. [38] explored the method of self-focusing a high-intensity array of femtosecond laser beams to enable efficient parallel laser surface processing at the millimeter scale. This method provided insight into the corrosion behavior of materials subjected to such processing, as superhydrophobic properties have been extended to multiple metallic substrates via ablation process. From the study, both the treated and untreated aluminum alloy were used to evaluate the material in an accelerated corrosion fog chamber. The FLSP-treated sample experienced pitting corrosion more quickly than the untreated sample during the accelerated corrosion tests, eliminating the FLSP treatment from the surface. Although this material has considerable hydrodynamic advantages, the enhanced rates of corrosion raise questions regarding the durability of this surface treatment [38]. FLSP is associated with various surface processing parameters that can be altered to produce different surface structures. It was proven that aluminum surfaces could

emit light in an almost pristine, broadband, and omni-directional fashion by the manipulation of the following parameters: pulse count, fluence, and ambient environment. This process yields functionalized metallic surfaces ideal for cutting-edge applications such as passive radiative cooling [39].

2.1.1 Advantages of femtosecond lasers over other laser types in surface processing applications

Femtosecond laser technology has shown great ability in the transformation of several surface processing methods. The technology is linked with the following advantages.

- High Precision and Resolution: Submicron-scale material removal and alteration are made possible because of femtosecond lasers' ultrashort pulse length. The microfabrication and nanotechnology industries particularly benefit from this great precision. Her et al. [40] showed how to fabricate silicon microstructures with submicron features using a femtosecond laser.
- Femtosecond lasers take advantage of nonlinear optical phenomena including multiphoton absorption, which gives them special processing abilities. Complex surface structures and material alterations can be created more easily because of these effects [41]. This method of processing has paved the way for the development of cutting-edge optical technologies including waveguides, micro-optics, and photonic crystals, enhancing optical communication and sensing technologies. As evidence of this potential, Nolte et al. [42] explored the development of photonic structures in glass and also waveguide creation in glass substrates was studied by Zhang et al [43].
- Reduced Material Damage: The absence of prolonged laser-material interaction in femtosecond pulses means less material damage and reduced risk of microcracking. This

property is crucial for preserving material integrity, as emphasized by Gan Yuan et al. [44]. This attribute makes the application suitable for delicate materials.

- Broad Material Compatibility: Femtosecond lasers are compatible with an extensive array of materials, encompassing metals, semiconductors, polymers, and transparent substrates. This versatility accommodates a diverse spectrum of surface processing applications applicable across various industries.
- Ultrafast Dynamics: Femtosecond lasers enable the observation and manipulation of ultrafast material dynamics. These capabilities open doors to novel processing techniques and offer insights into fundamental laser-material interactions [45].
- Femtosecond lasers are used in biomedical sectors like tissue engineering and ophthalmology where accuracy and little tissue damage are key requirements. Femtosecond laser-assisted cataract surgery was illustrated by Palanker et al. [46].

2.2 Component Parts of FLSP

A femtosecond laser, like any other laser, consists of several key components that work together to generate ultra-short pulses of laser light. These components typically include:

Gain Medium: The gain medium is the material (often a solid-state crystal or fiber) that amplifies the light through stimulated emission. In the case of femtosecond lasers, the gain medium must be able to support ultra-short pulse durations.

Laser Cavity: The laser cavity consists of two mirrors (one partially reflecting and one fully reflecting) that form a resonant cavity. The gain medium is placed within this cavity.

Pulse Shaping Elements: Femtosecond lasers often employ pulse shaping elements such as prisms, gratings, or acousto-optic modulators to shape the output pulse and compress it to the femtosecond scale.

Mode-Locking Mechanism: Mode-locking is a crucial process in femtosecond lasers that synchronizes the phases of different longitudinal modes of the laser, resulting in ultra-short pulse generation. This can be achieved through techniques like Kerr-lens mode-locking or semiconductor saturable absorber mirrors.

Pump Source: The gain medium in femtosecond lasers is typically pumped with an external source, such as a continuous-wave laser or a flash lamp.

Beam Steering and Scanning Optics: Optical components like mirrors, lenses, and beam splitters are used to control the direction and focus of the laser beam.

Output Coupler: The partially reflecting mirror in the laser cavity acts as the output coupler, allowing a portion of the laser light to exit the cavity as the laser output.

Pulse Compression Components: Femtosecond lasers often incorporate dispersion compensation elements like prisms or gratings to compress the output pulses, which are initially chirped, into ultra-short, nearly transform-limited pulses.

Cavity Stabilization Mechanisms: Keeping the laser cavity stable and precisely aligned is crucial for maintaining the short pulse duration.

Control and Monitoring Electronics: Electronic systems for controlling laser parameters and monitoring performance, including factors like pulse duration and repetition rate.

These components work together to produce femtosecond laser pulses, which have durations on the order of femtoseconds (10^-15 seconds) and are used in a wide range of scientific, medical, and industrial applications, including ultrafast spectroscopy, material processing, and medical procedures. Figure 4 shows a schematic of the laser processing configuration.

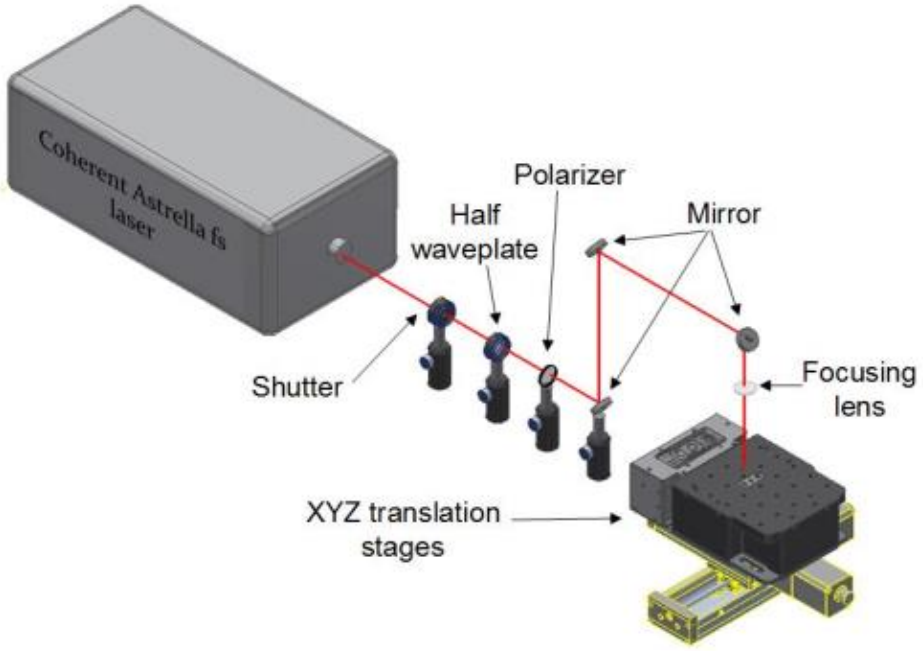

Figure 4. Schematic of the laser processing setup.

CHAPTER 3

APPLICATIONS OF FEMTOSECOND LASER PROCESSED AND NANONEEDLE SYNTHESIZED SURFACES TO ENHANCE POOL BOILING HEAT TRANSFER

3.1 Surface Preparation

The creation and characterization of samples, as well as explanations of the cleaning process using citric acid, the nanoneedle production method, and the heat treatment process, are covered in the sections that follow.

3.1.1 FLSP Technique

FLSP illuminates metallic surfaces with an extremely fast laser to produce intricate micro- and nanostructures on the surfaces. The laser fluence and quantity of laser pulses on the substrate determine the shape and physical properties of these structures. These physical properties include the thickness of the nanoparticle layer, the microstructure spacing, and the peak to valley height [18, 6]. In this investigation, the same laser parameters were used to create each FLSP sample, resulting in an identical underlying morphology that allowed the impacts of the hybrid nanoneedle method to be assessed.

To achieve stable structures in this study, a Coherent Astrella Ti:sapphire femtosecond laser, operated at a central wavelength of 800 nm and generating 6 mJ of energy, was employed for sample generation. The pulse duration of each femtosecond pulse was temporarily extended to 4 ps by adjusting the compressor of laser pulse [47].

The energy in each pulse was 3200 μJ, and it was supplied at a frequency of 1 kHz. The incident beam was focused on the surface of the copper substrate by means of a 150 mm plano-convex lens.

Additionally, the following laser parameters were utilized to fabricate all the samples used for this test; a stage velocity of 10 mm/s, a raster pitch of 40 µm, a pulse count of 700, a Gaussian spot diameter of 600 µm, and a laser peak fluence of 2.26 J/cm^2.

3.1.2 Citric Acid Cleaning

After laser processing on some of the fabricated samples, citric acid was used to clean the surface in order to eliminate oxides from the samples that developed during the FLSP process. These oxides tend to have a negative impact on the boiling efficiency of FLSP-processed copper samples [18, 19]. Dipping the samples in citric acid that had been diluted to 0.5 M for a duration of 5 minutes assisted in taking the oxides off the copper samples with no impact on the characteristics of the sample [19]. Following the acid cleaning, the FLSP surface underwent a 25-minute ultrasonic bath in ethanol to ensure the removal of any residual citric acid. To completely evaporate any remaining ethanol, the samples were lastly, dried using nitrogen.

3.1.3 Nanoneedle Synthesis

On the fabricated surfaces, nanoneedles were synthesized by employing a method similar to Zhang et al. [48]. The following method was used to create a solution of ammonium persulfate ($(NH4)_2S_2O_8$) and sodium hydroxide ($NaOH$) utilized to commence synthesis. To produce this solution, 20 mL of NaOH and 40 mL of nanopure water were first mixed. Then, more Nanopure water was added until a volume of 150 mL was attained. The resulting solution was then mixed with 3.42 grams of ($(NH4)_2S_2O_8$) powder containing not more than 98% ACS reagent until it turned transparent. To give the nanoneedles time to form, the samples were submerged in the solution for 5 minutes. Following synthesis, to stop the reaction, the samples were first immersed in a beaker of Nanopure water, and then dried with nitrogen. Copper hydroxide had formed, as shown by the

blue color of the finished surfaces. The production of the copper hydroxide nanoneedles is described by the following reaction [48]:

$$Cu + 4NaOH + (NH4)_2S_2O_8 \rightarrow Cu(OH)_2 + 2Na_2SO_4 + 2NH_3 \uparrow + 2H_2O \quad (1)$$

3.1.4 Heat Treatment

It was observed that the nanoneedles were not properly bonded to the copper substrate as the needles disappeared during the degassing process. To prevent this occurrence, a furnace was used to heat treat 4 of the fabricated samples.

The furnace used for the heat treatment process was a vacuum oven (ACCUTEMP-19) which has a temperature range from ambient to 670^{o}F (354^{o}C) and utilizes atmospheric pressure. It took about 1 hour 30 minutes of heating for the sample to get to 200^{o}C and further heating was done at 200^{o}C for 30 minutes. The sample was allowed to cool in the furnace and then brought out and stored in nitrogen.

3.1.5 Boiling Surfaces and Characterization

Keyence: VK-X200 laser scanning confocal microscopy (LSCM) was first used to evaluate each surface to get numerical data. The nanoneedles reduced size prevented LSCM data from being obtained for the surfaces of the nanoneedles after synthesis. The LSCM system employed utilizes a laser with a wavelength of 408 nm and was incapable of completely resolving submicron-scale features. This limitation resulted in unrealistic measurements of the sample morphology. Consequently, morphology data for samples containing nanoneedles (samples D and E) are not presented in Table 2. Table 2 outlines the procedure used in the fabrication of each sample.

*Table 2**: LSCM Data and samples fabrication steps.*

Sample	Fabrication Steps	Structure Height, R_z (µm)	Average Roughness R_z (µm)	Surface Area Ratio SA/A
Polished		1.0 ± 0.3	0.07 ± 0.02	1.1
D	FLSP + NNS + NNS	- - -	- - -	- - -
E	FLSP + CAC + NNS + HT	- - -	- - -	- - -

Abbreviations: femtosecond laser surface processing (FLSP); citric acid cleaning (CAC); nanoneedle synthesis (NNS): heat treatment (HT).

The next step was to use the FEI Helios Nanolab 660 Dual-beam system scanning electron microscope (SEM) to obtain the characteristics and general shape of the sample and to obtain high-quality images of the copper hydroxide nanoneedles. Copper hydroxide nanoneedles were visible and spreading throughout the whole surface. SEM images were taken before and after the heat treatment of the nanoneedles samples to confirm the presence of nanoneedles after the heat treatment process. Figure 5 below are images of the sample under SEM images before and after the heat treatment process. The nanoneedles were no longer straight after the heat treatment process.

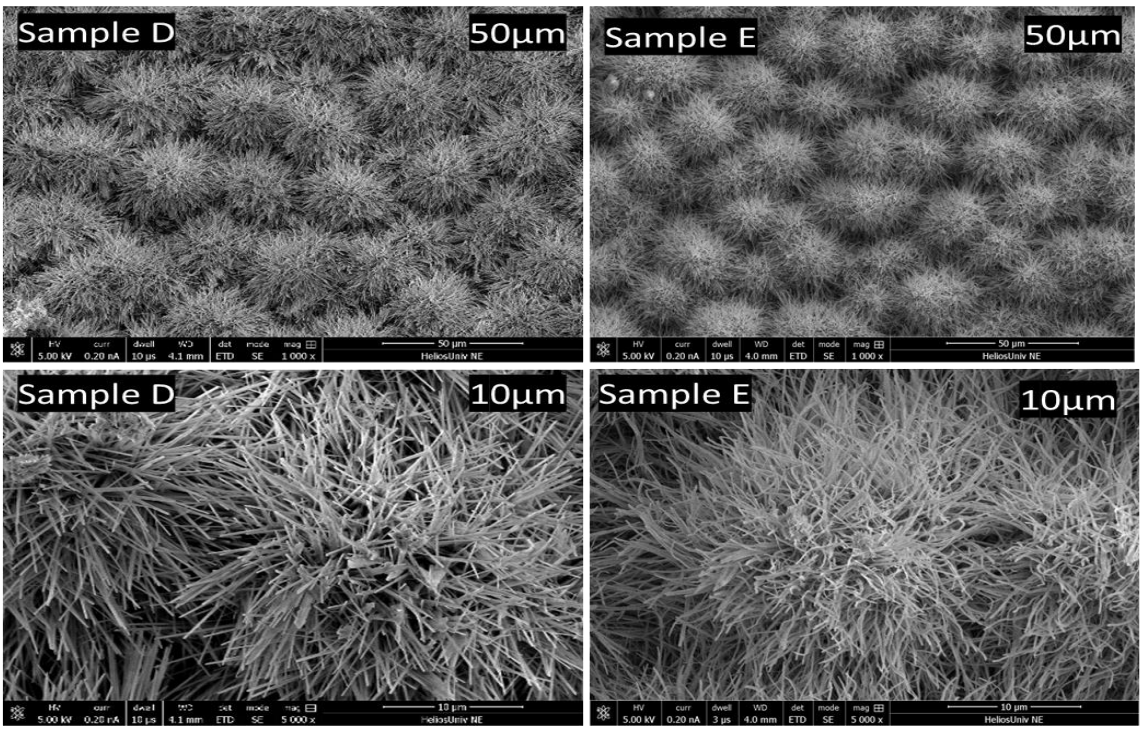

Figure 5. SEM images of nanoneedles sample; D (before heat treatment), and E (After heat treatment).

Table 3 below is a summary of all fabricated samples used.

*Table 3**: Summary of fabricated samples**.*

SAMPLE NUMBER	DATE PRODUCED	FABRICATION STEPS	USE	REMARK
1	7/10/2022	FLSP+CAC+NNS	Degassing	Nanoneedles disappeared after degassing
2	7/10/2022	FLSP+CAC+NNS+HT	Pool Boiling	The sample was heated in a furnace at 200°C
3	7/10/2022	FLSP+CAC+NNS	Degassing	Nanoneedles disappeared after degassing
4	7/10/2022	FLSP+CAC+NNS+HT	Pool Boiling	The sample was heated in a furnace at 200°C
5	7/10/2022	FLSP+CAC+NNS	Not Used	Nanoneedles still present
6	7/10/2022	FLSP+CAC+NNS	Turned Black(Not Used)	No Nanoneedle found on the surface after SEM
7	11/22/2022	FLSP+CAC+NNS+HT	Pool Boiling	The sample was heated in a furnace at 200°C
8	11/22/2022	FLSP+CAC+NNS+HT	Pool Boiling	The sample was heated in a furnace at 200°C

3.2 Pool Boiling Experimental Setup and Methods

The test setup for pool boiling includes a chamber made of aluminum resembling the one used by Costa-Greger et al [31]. Several working fluids can be used with the experimental setup. Figure 6 below depicts the pool boiling test setup. The test apparatus included the test sample (boiling surface), a liquid reservoir with a capacity of around 8 liters of DI water, and a base heater to generate the heat flux required. A piece of McMaster: 8965K45 101 copper was fabricated to a diameter of 25.4 mm to form the samples. After functionalizing the sample, the sample was then forced into a high-performance semi-crystalline engineering thermoplastic lining called polyetheretherketone (PEEK) to avoid heat loss across the radius throughout the pool boiling

process.. Five Omega TJ36-CASS-032G-6 K-type thermocouples having a precision of ±1.1 °C were then inserted into five equally spaced holes in the sample. The sample's perimeter was coated with a two-component McMaster: 7556A33 epoxy was applied to mitigate premature nucleation at the sample's edges. Epoxy was also used to hold all 5 thermocouples in place and for the complete sealing of the pool boiling setup at the contact between the aluminum enclosure and PEEK lining to prevent leakage.

Before attaching the acrylic front panel, silicone glue was next applied to the whole chamber's front face. The epoxy and silicone glue were allowed to completely bond the night before the experiment was conducted.

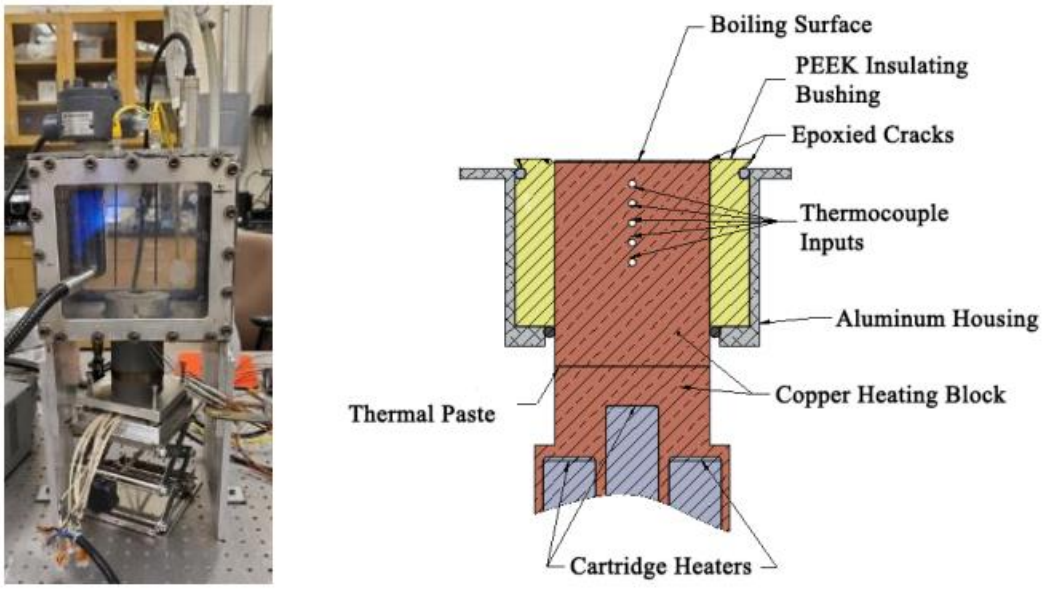

Figure 6. Left - Complete pool boiling test setup, Right - Cross section of test setup showing the major parts, installed sample and thermocouple locations.

The pool boiling experiment started by filling the chamber with distilled water. The immersion heater was turned on to bring the working fluid to its saturation temperature. Also, the chiller was turned on to control the temperature. The deionized (DI) water was permitted to aggressively boil

for 60 minutes after reaching saturation temperature to eliminate any residual gases. A water-cooled reflux condenser took out the vapor produced by the immersion heater which was connected to the chiller and fixed atop the pool boiling setup. This kept the operational pressure close to atmospheric pressure and the system mass fixed, respectively. An Omega PX409- 030A5V pressure transducer placed atop the experimental setup helped in tracking ambient pressure. Following degassing, McMaster 3715N11 thermal paste was applied to the top surface of the base heater which was in contact with the base of the sample. The purpose of this paste was to aid efficient heat transfer from the base heater to the sample. A laboratory jack was used to connect the base heating block to the sample's base. To compensate for any misalignment between the heating surfaces, the laboratory jack and the base heating block were separated by an extensible spring plate. Then, a parallel connection of five cartridge heaters each rated for 500 Watts and 120 volts was created, and an analog voltage transformer was utilized to power the heaters. The voltage transformer was first adjusted to 20 Volts to get the initial reading, and for subsequent data points the voltage was raised by 5 Volts. K-type thermocouples were used to measure temperatures at 5 evenly separated points throughout the sample's axis with an accuracy of ±1.1 °C. LabVIEW was used to monitor and gather data in order to document the constant and time dependent performance. To decide when to capture data, a steady state criterion was used with the rate of change of temperature of 0.25 °C/min like that used by Costa-Greger et al [31]. Discrete derivatives were computed between consecutive points by utilizing the data gathered at a frequency of 1.25 Hz. The average of these derivatives was then calculated throughout a shifting three-minute window. Data was captured for a duration of two minutes, averaged, and then used to create the boiling curves once the steady state requirement had been fulfilled and sustained for at least five minutes. This procedure was repeated with a 5 Volts increase in voltage until there

was an abrupt temperature increase accompanied by corresponding reduction in the rate of heat transferred per unit area which signified attainment of CHF. The average of the transient data for the previous 30 seconds before the temperature rise was used to obtain the CHF.

3.2.1 Surface Temperature and Heat Flux Calculation

A one-dimensional conduction model was utilized to determine the surface temperatures and heat flux from temperatures measured by five evenly separated points across the axis of the copper block. Using equation (2) below, heat fluxes between several thermocouple pairs were calculated:

$$q_{ij}'' = -k\frac{T_i - T_j}{x_{ij}} \tag{2}$$

T_i and T_j denote the thermocouples temperatures, q is the heat flux, k denotes the thermal conductivity of the copper sample which is 400 W/m-K and was assumed to be constant, x denotes the space between the thermocouples, and i and j denote the different thermocouples.

Assuming that the thermocouples are numbered 1 through 5, the actual heat flux was determined from the estimated heat fluxes by pairing the thermocouples. The pairing formats used are as follows: 1 and 3, 2 and 4, 3 and 5, and 1 and 5. The distance between two consecutive thermocouples is 3.18 mm, resulting in thermocouple gaps of 6.36 mm for the initial three pairs and 12.72 mm for the final pair. By applying the formula in equation (3) below, surface temperatures were predicted utilizing the actual heat flux and the temperature recorded closest to the surface:

$$T_s = T_1 - q''\frac{x_1}{k} \tag{3}$$

T_s and T_1 are the sample surface temperature and the temperature measured near the sample surface, q'' denotes the actual heat flux, and x_1 denotes distance measured from the last thermocouple to the sample surface which was 4.50 mm.

A pressure transducer located atop the pool boiling test setup was used to record the pressures within the pool boiling chamber and these pressures were utilized to estimate the saturation temperature during the boiling process. Equation (4) was used to obtain the HTC denoted by h. T_{sat} is the saturation temperature of the liquid used for this experiment.

$$h = \frac{q''}{T_s - T_{sat}} \tag{4}$$

3.2.2 Uncertainty Evaluation

The conventional error propagation equation was employed to estimate the uncertainties for both the surface temperatures and the heat flux. According to the accuracy of the measurement tools, 4%, 1.2 °C, and 6% discrepancy in the heat flux, superheat, HTC at CHF respectively. **Error! Reference source not found.** below shows the measured and calculated uncertainty values.

$$\delta q''_{ij} = \sqrt{(\frac{\partial q''_{ij}}{\partial T_i}\delta T_i)^2 + (\frac{\partial q''_{ij}}{\partial T_j}\delta T_j)^2 + (\frac{\partial q''_{ij}}{\partial x_{ij}}\delta x_{ij})^2} \tag{5}$$

$$\delta T_s = \sqrt{(\frac{\partial T_s}{\partial T_1}\delta T_1)^2 + (\frac{\partial T_s}{\partial q''}\delta q'')^2 + (\frac{\partial T_s}{\partial x_1}\delta x_1)^2} \tag{6}$$

Table 4. Summary of uncertainties at critical heat flux.

Parameter	Uncertainty

Temperature, Ti, Tj	± 1.1 °C
Thermocouple spacing, xij	± 0.15 mm
Distance from surface to top thermocouple, $x1$	± 0.08 mm
Heat flux, q"	± 4 %
Surface temperature, Ts	± 1.2 °C
Heat transfer coefficient, h	± 6 %

CHAPTER 4

4.1 Results and Discussion

Several samples were used for pool boiling experiments and the results were compared to investigate the repeatability of the process. The result analysis followed the generation of boiling curves up to the CHF for each specimen with a polished surface as reference to compare the performance of the processed samples. Figure 7 depicts a boiling curve which showed a comparison of the results obtained from the four different runs of sample 2 (FLSP+CAC+NN+HT) with a polished reference Surface. The sample was not removed from the pool boiling chamber until after the last run to prevent the result alteration arising from removal and installation of sample. It was observed that all runs with sample 2 followed a similar pattern. The boiling curves for all 4 runs of sample 2 are shifted to the right of the boiling curve that corresponds to the polished surface. The last 3 runs produced very similar results however, the first run showed a slight deviation to the right. The 3 clustered runs of sample 2 almost coincided with the non-heat-treated nanoneedle sample (FLSP+CAC+NN) fabricated by Costa-Greger et al. [31]. All runs with Sample 2 are to the right of the polished surface which showed a reduced performance of the processed samples. The maximum CHF obtained with sample 2 was 116.1 W/cm^2 with an HTC of 50.5 kW/m^2-K at wall superheat of 23 ^{o}C. This corresponds to 6.4 % and 2.5 % reduction in CHF and HTC respectively when compared to polished copper surface which generated a CHF of 124 W/cm^2 and an HTC of 51.8 KW/m^2-K.

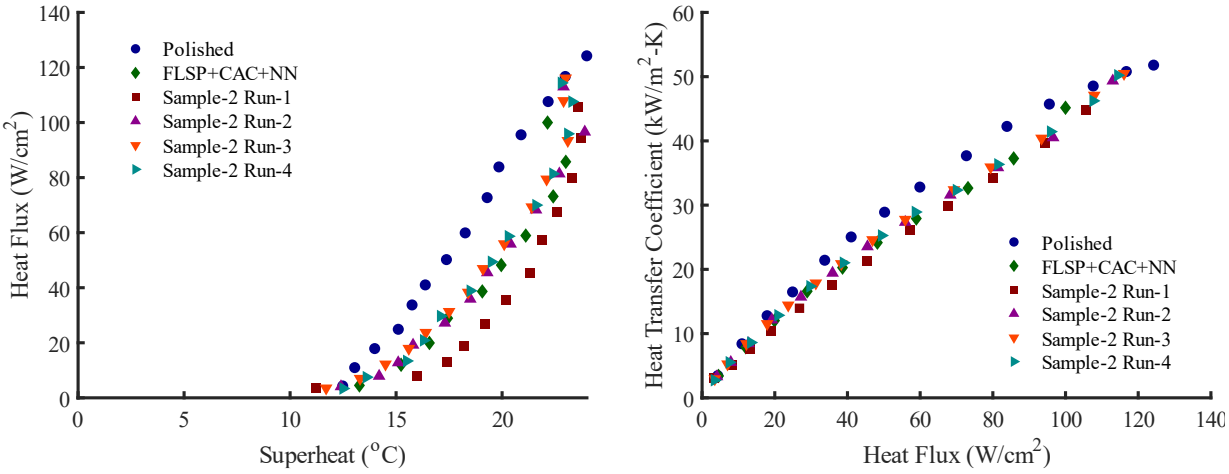

Figure 7. Boiling curve which shows a comparison of Sample 2 with Polished reference Surface.

A boiling curve comparison of two runs of sample 4 (FLSP+CAC+NN+HT) with polished reference surface is shown in Figure 8. A maximum CHF value of 115.3 W/cm^2 was attained with a corresponding HTC of 50.8 kW/m^{2}K at a superheat of 22.7 ^{o}C. The sample experienced a boiling inversion at a superheat of 24.4 ^{o}C. From the second run with Sample 4, a CHF of 95 W/cm^2 was attained with a corresponding HTC of 42 kW/m^{2}K at a superheat of 22.6 ^{o}C. Compared to the boiling curve of the first run, the boiling curve of the second run shifted to the left. This difference could be attributed to the removal and reinstallation of the sample.

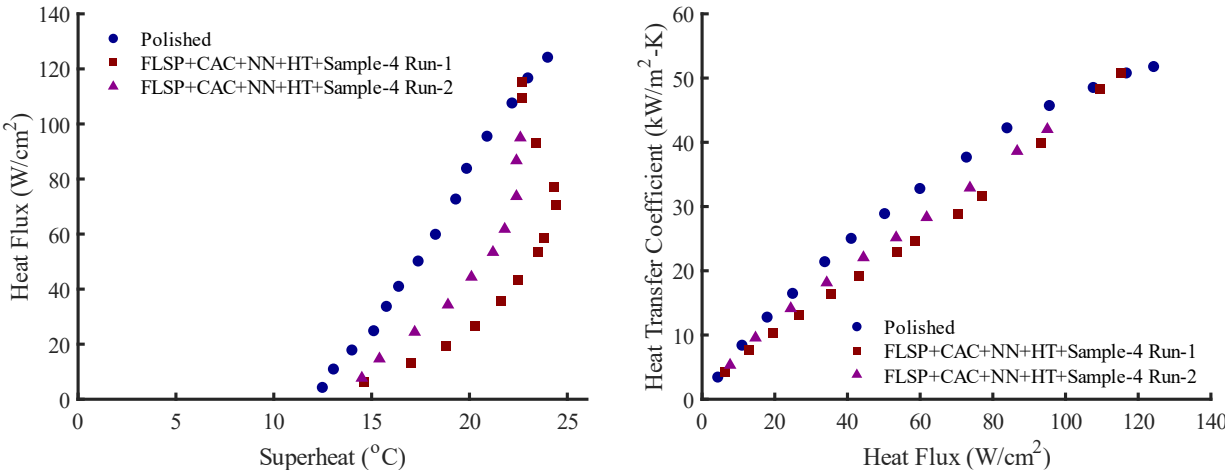

Figure 8. Boiling curve which shows a comparison of Sample 4 with Polished reference Surface.

Figure 9 shows a comparison between the four runs of sample 8 (FLSP+CAC+NN+HT) and a run of the polished reference surface. A shift of the boiling curve to the left was observed after every consecutive run. The difference between the results obtained for the 3rd and 4th pool boiling runs is very minimal. This difference in results may be because of removing and installing the sample before and after each run as earlier stated. A maximum CHF of 109.2 W/cm^2 was attained with a corresponding HTC of 51.5 kW/m2K at a superheat of 21.2 ^{o}C.

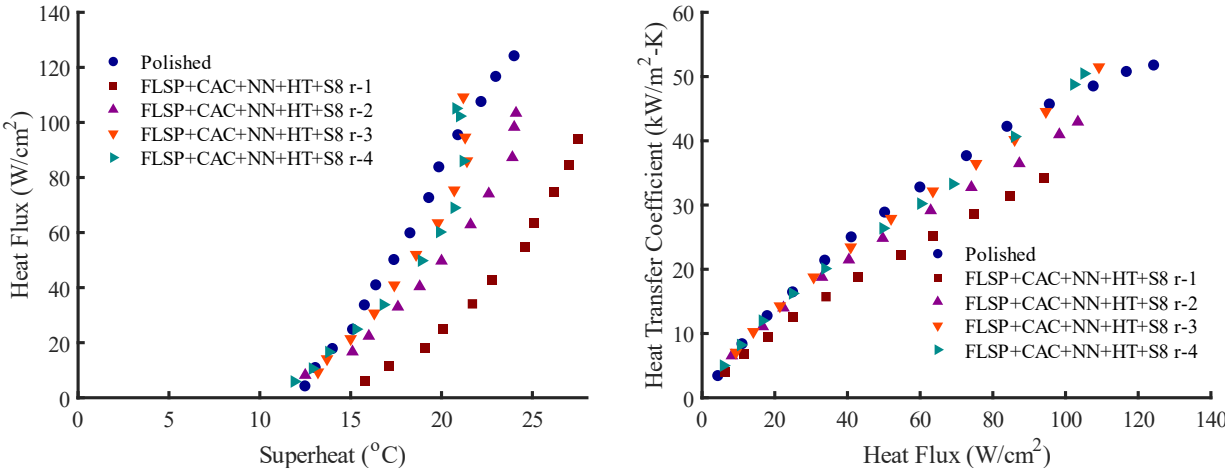

Figure 9. Boiling curve which shows a comparison of Sample 8 with Polished reference Surface.

The Figure 10 compares the boiling curve of all processed samples, the polished copper surface used in this study and with the nanoneedle sample presented by Costa-Greger et al. [31]. The boiling curves of all the processed samples are to the right of the boiling curve that corresponds to the polished reference surface. Both samples 2 and 8 are to the left of the sample (FLSP+CAC+NN) used in [31], which shows that the heat treatment of those samples (FLSP+CAC+NN+HT) enhanced the heat transfer performance. This enhancement could be due to the heat treatment preventing the removal of the nanoneedles from the sample surface. The processed surfaces experienced boiling inversion and demonstrated a shift to the left of the boiling

curve after each successive run, illustrating an enhancement. Stability was observed after the second run as results obtained after this run were almost the same.

For the (FLSP+CAC+NN+HT) samples, the maximum CHF of 116.1 W/cm^2 was obtained with sample 2 at an HTC of 50.5 kW/m^2-K at wall superheat of 23°C.

This corresponds to a 6.4% reduction in CHF and a 2.5% reduction in HTC when compared to the polished copper surface, which has a CHF of 124 W/cm^2 and an HTC of 51.8 kW/m^2-K. The results are summarized in Table below.

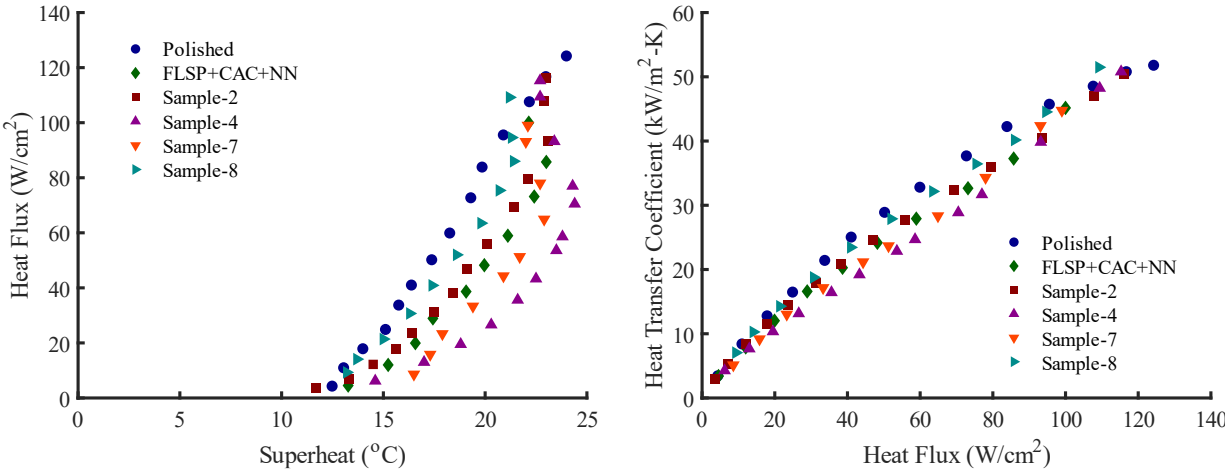

Figure 10. Boiling Curves comparing all processed samples with a polished copper surface.

Table5: Summary of pool boiling performance.

Sample	Process Steps	CHF (W/cm^2)	HTC (KW/m^2-K)
Polished	-	124	51.8
D	FLSP+CAC+NNS	100 (-20%)	45.2 (-13%)
E	FLSP+CAC+NNS+HT	116.1(-6.4%)	50.5 (-2.5%)

Abbreviations: FLSP, femtosecond laser surface processing; CAC, citric acid cleaning; NNS, nanoneedle synthesis; HT, Heat Treatment.

4.1.1 Durability of Nanoneedle

Finally, an assessment of the nanoneedles' durability was performed by taking SEM images of each hybrid sample (FLSP + nanoneedle synthesis) both before and after the boiling experiments.

The outcomes are illustrated in Figure 11. Before pool boiling experiments with the nanoneedle samples, it was observed from SEM images that the nanoneedles disappeared after degassing process. The heat treatment of the sample helped to retain the nanoneedles on the surface of the samples, as the $Cu(OH)_2$ nanoneedles were still present after several pool boiling runs. Although, the needles were no longer straight after the heat treatment process.

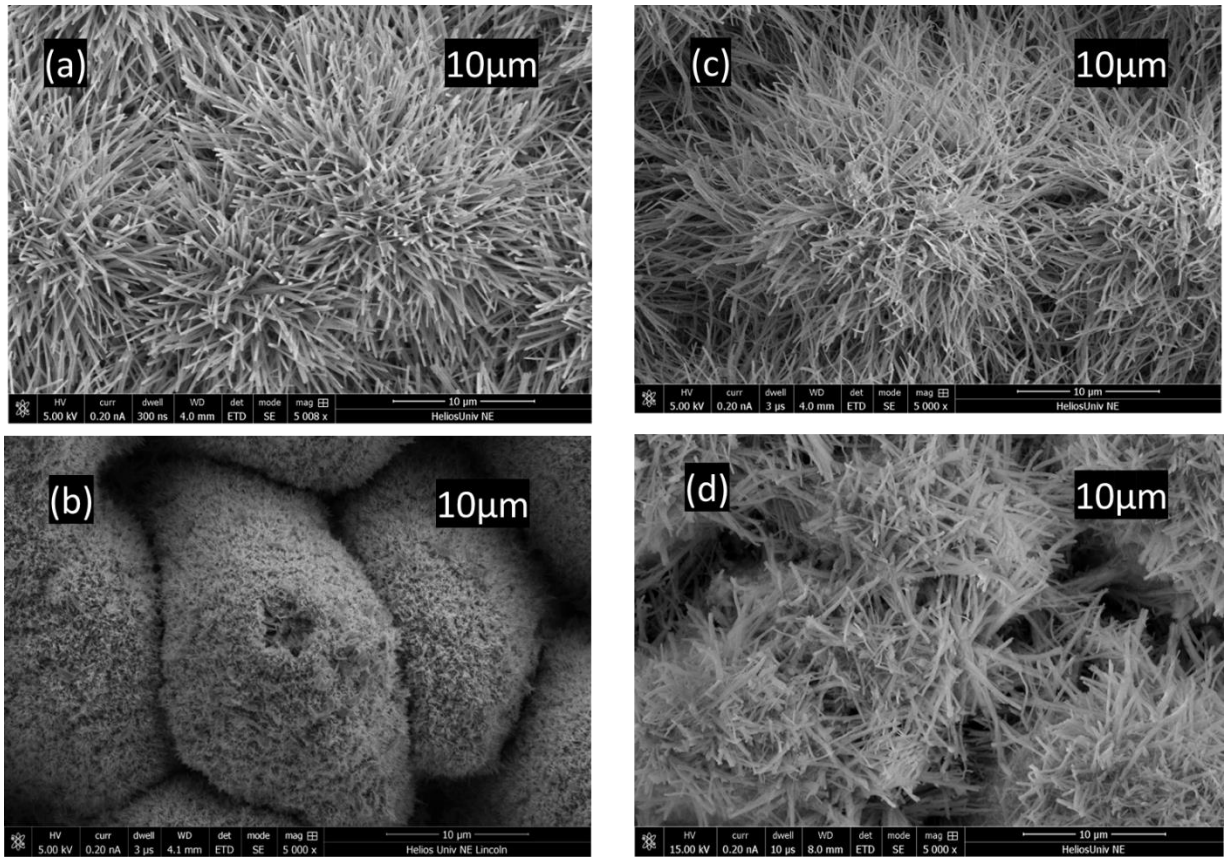

Figure 11. Before and after pool boiling experiments with the nanoneedle sample, (a) sample D before boiling, (b) sample D after boiling, (c) sample E before boiling, and (d) sample E after boiling.

CHAPTER 5

5.1 Conclusion

This study examines the pool boiling performance of copper hydroxide $Cu(OH)_2$ nanoneedle surface which was heat treated (Sample E) to help retain the nanoneedles during pool boiling process. The heat-treated sample was then compared to a nanoneedles sample that was not heat treated (Sample D). The following conclusions can be drawn:

1. Comparatively, both samples D and E exhibited elevated superheats and reduced Heat Transfer Coefficients (HTCs) of 13 % and 2.5 %, respectively, when compared with the polished reference surface. It is noteworthy that these observations persisted even after applying a citric acid cleaning process to eliminate underlying oxidation.
2. Sample E (FLSP+CAC+NN+HT) with a CHF of 116.1 W/cm^2 at an HTC of 50.5 kW/m^2-K outperformed sample C (FLSP+CAC+NN) which has a CHF of 100 W/cm^2 at an HTC of 45.2 kW/m^2-K.
3. Scanning electron microscopy (SEM) images captured before and after the boiling experiments on hybrid surfaces E demonstrate that the heat treatment process played a vital role in anchoring the nanoneedles securely in place. This, in turn, contributed to the enhanced performance exceeding that of sample C.
4. The results obtained showed that there was repeatability.

5.2 Recommendations

The $Cu(OH)_2$ nanoneedles should undergo heat treatment at various temperatures and subsequently be employed in pool boiling experiments. The variation in heat treatment temperatures would be used to determine if further enhancement in heat transfer performance can still be attained. Other methods of securing the nanoneedles to the copper surface can also be explored.

REFERENCES

[1] Han, C.Y., Griffith, P., "The mechanism of heat transfer in nucleate pool boiling—part I," *Int. J. Heat Mass Transfer,* vol. 8, no. 6, p. 887–904, 1965.

[2] Ji, Q., Chen, X., Liang, J., Laude, V., Guenneau, S., Fang, G. and Kadic, M., " Designing thermal energy harvesting devices with natural materials through optimized microstructures," *International Journal of Heat and Mass Transfer,* vol. 169, p. 120948, 2021.

[3] Jung, K.W., Kharangate, C.R., Lee, H., Palko, J., Zhou, F., Asheghi, M., Dede, E.M. and Goodson, K.E, "May. Microchannel cooling strategies for high heat flux (1 kW/cm 2) power electronic applications," *16th IEEE Intersociety Conference on Thermal and Thermomechanical Phenomena in Electronic Systems (ITherm),* pp. 98-104, 2017.

[4] Liang, G. and Mudawar, I., "Review of pool boiling enhancement by surface modification," *International Journal of Heat and Mass Transfer,* vol. 128, pp. 892-933, 2019.

[5] Sen, P., Kalita, S., Sen, D., Das, A.K. and Saha, B.B., "Pool boiling heat transfer and bubble dynamics of modified copper micro-structured surfaces," *International Communications in Heat and Mass Transfer,* vol. 134, p. 106039, 2022.

[6] Kruse, C.M., Anderson, T., Wilson, C., Zuhlke, C., Alexander, D., Gogos, G. and Ndao, S. , "Enhanced pool-boiling heat transfer and critical heat flux on femtosecond laser processed stainless steel surfaces," *International journal of heat and mass transfer,* vol. 82, pp. 109-116, 2015.

[7] Thome, J.R. , New York,, "Enhanced Boiling Heat Transfer," *Hemisphere Pub. Corp.,.*

[8] Bergles, A.E. , "Techniques to Enhanced Heat Transfer, third," *Handbook of Heat Transfer,* p. 11.1–11.76, 1998.

[9] Bergles, A.E., Bakhru, N., Shgires, J.W., "Cooling of high power density computer components," *MIT Engineering Project Laboratory (DSR 70712-60),* 2004.

[10] Webb, R.L. , "Principles of Enhanced Heat Transfer," *second ed., Wiley-Interscience,,* 1994.

[11] Gajghate, S.S., Bandurkar, A.V., Das, S., Saha, B.B. and Bhaumik, S., , "Effect of ZrO2 nanoparticle deposited layer on pool boiling heat transfer enhancement," *Heat Transfer Engineering,* Vols. 13-14, no. 42, pp. 1184-1202, 2021.

[12] Jones, B.J., McHale, J.P., Garimella, S.V. , "The influence of surface roughness on S.V. nucleate pool boiling heat transfer," *J. Heat Transfer ,* vol. 131, no. 12, p. 1009, 2009.

[13] Bergles, A.E., Chyu, M.C. , "Characteristics of nucleate pool boiling from porous metallic coatings," *J. Heat Transfer,* vol. 104, no. 2, p. 270, 1982.

[14] Borzenko, V.I., Malyshenko, S.P., , "Mechanisms of phase exchange under conditions of boiling on surfaces with porous coatings," *High Temp. ,* vol. 39, no. 5, p. 714–721, 2001.

[15] Li, C., Peterson, G.P. , "Parametric study of pool boiling on horizontal highly conductive microporous coated surfaces," *J. Heat Transfer,* vol. 129, no. 11, p. 1465, 2007.

[16] Saeidi, D., Alemrajabi, A. A. and Saeidi, N., "Experimental study of pool boiling characteristic of an aluminized copper surface," *International Journal of Heat and Mass Transfer,* vol. 85, pp. 239-246, 2015.

[17] Može, M., Zupančič, M., Hočevar, M., Golobič,I. and Gregorčič, P., "Surface chemistry and morphology transition induced by critical heat flux incipience on laser-textured copper surfaces," *Appl. Surf. Sci.,,* vol. 490, p. 220–230, October 2019.

[18] Kruse, C. et al., "Influence of Copper Oxide on Femtosecond Laser Surface Processed Copper Pool Boiling Heat Transfer Surfaces," *Journal Heat Transfer,* vol. 141, no. 5, p. 051503, May 2019.

[19] Anderson, M. et al.,, "Heat transfer behavior of as-processed and cleaned picosecond pulse laser processed copper," *Therm. Sci. Eng. Prog,* vol. 27, p. 101105, January 2022.

[20] Mani, D., Sivan, S., Ali, H. M. and Ganesan, U. K., "Investigation to Improve the Pool Boiling Heat Transfer Characteristics Using Laser-Textured Copper-Grooved Surfaces," *Int. J. Photoenergy,* pp. 1-8, Feburary 2020.

[21] Das, S., Kumar, D.S. and Bhaumik, S., "Experimental study of nucleate pool boiling heat transfer of water on silicon oxide nanoparticle coated copper heating surface. Applied Thermal Engineering," vol. 96, pp. 555-567, 2016.

[22] Shi, B., Wang, Y.-B. and Chen, K. , "Pool boiling heat transfer enhancement with copper nanowire arrays," *Appl. Therm. Eng,* vol. 75, p. 115–121, January 2015.

[23] Yang, Y., Ji, X., and Xu, J., "Pool boiling heat transfer on copper foam covers with water as working fluid," *Int. J. Therm. Sci.,,* vol. 49, no. 7, p. 1227–1237, July 2010.

[24] Jaikumar, A. and Kandlikar, S.G. , "Enhanced pool boiling heat transfer mechanisms for selectively sintered open microchannels," *International Journal of Heat and Mass Transfer,* vol. 88, pp. 652-661, 2015.

[25] Rishi, A.M., Kandlikar, S.G. and Gupta, A. , "Improved wettability of graphene nanoplatelets (GNP)/copper porous coatings for dramatic improvements in pool boiling heat transfer," *International Journal of Heat and Mass Transfer,* vol. 132, pp. 462-472, 2019.

[26] Wang, X., Fadda, D., Godinez, J., Lee, J. and You, S.M., " Effect of wettability on pool boiling heat transfer with copper microporous coated surface.," *International Journal of Heat and Mass Transfer,* vol. 194, p. 123059, 2022.

[27] Rishi, A.M., Gupta, A. and Kandlikar, S.G., "Improving aging performance of electrodeposited copper coatings during pool boiling," *Applied Thermal Engineering,* vol. 140, pp. 406-414, 2018.

[28] MacNamara, R.J., Lupton, T.L., Lupoi, R. and Robinson, A.J. , "Enhanced nucleate pool boiling on copper-diamond textured surfaces," *Applied Thermal Engineering,* vol. 162, p. 114145, 2019.

[29] Jaikumar, A., Rishi, A., Gupta, A. and Kandlikar, S.G., "Microscale morphology effects of copper–graphene oxide coatings on pool boiling characteristics," *Journal of Heat Transfer,* vol. 139, no. 11, p. 111509., 2017.

[30] Munonyedi Egbo, Mohammad Borumand, Yahya Nasersharifi, Gisuk Hwang, "Review: Surface orientation effects on Pool-boiling with plain and enhanced surfaces," *Applied Thermal Engineering,* vol. 204, p. 117927, 2022.

[31] Costa-Greger, J., Damoulakis, G., Kaufman, G., Sarin, S., Pettit, C., Shield, J., Megaridis, C., Zuhlke, C. and Gogos, G., "Pool Boiling Performance of Surfaces Produced by Femtosecond Laser Surface Processing and Copper Hydroxide Nanoneedle Growth," *IEEE Intersociety Conference on Thermal and Thermomechanical Phenomena in Electronic Systems,* pp. 1-10, 2022.

[32] Bonse, J., Höhm, S., Kirner, S.V., Rosenfeld, A. and Krüger, J., , "Laser-induced periodic surface structures—A scientific evergreen," *IEEE Journal of selected topics in quantum electronics,* vol. 23, no. 3, 2016.

[33] Palanker, D.V., Blumenkranz, M.S., Andersen, D., Wiltberger, M., Marcellino, G., Gooding, P., Angeley, D., Schuele, G., Woodley, B., Simoneau, M. and Friedman, N.J., , "Femtosecond laser–assisted cataract surgery with integrated optical coherence tomoggraphy," *Science translational medicine,* vol. 58, no. 2, pp. 58ra85-58ra85, 2010.

[34] Balling, P. and Schou, J.,, "Femtosecond-laser ablation dynamics of dielectrics: basics and applications for thin films," *Reports on progress in physics,* vol. 76, no. 3, p. 036502, 2013.

[35] Vorobyev, A.Y. and Guo, C., , "Direct femtosecond laser surface nano/microstructuring and its applications," *Laser & Photonics Reviews,* vol. 7, no. 3, pp. 385-407, 2013.

[36] "Superhydrophobic metallic surfaces functionalized via femtosecond laser surface processing for long term air film retention when submerged in liquid," *Craig A. Zuhlke, Troy P. Anderson, Pengbo Li, Michael J. Lucis, Nick Roth, Jeffrey E. Shield, Benjamin Terry, Dennis R. Alexander,* vol. 9351, 2015.

[37] Peng, E., Tsubaki, A., Zuhlke, C.A., Wang, M., Bell, R., Lucis, M.J., Anderson, T.P., Alexander, D.R., Gogos, G. and Shield, J.E., , "Micro/nanostructures formation by femtosecond laser surface processing on amorphous and polycrystalline Ni60Nb40," *Applied surface science,* vol. 396, pp. 1170-1176, 2017.

[38] Ley, J.R., Kwon, Y.W., Park, C. and Menon, S.K., , "Corrosion of femtosecond laser surface textured aluminium alloy," *Corrosion Engineering, Science and Technology,* vol. 52, no. 7, pp. 526-532, 2017.

[39] Reicks, A., Tsubaki, A., Anderson, M., Wieseler, J., Khorashad, L.K., Shield, J.E., Gogos, G., Alexander, D., Argyropoulos, C. and Zuhlke, C., , "Near-unity broadband omnidirectional emissivity via femtosecond laser surface processing," *Communications Materials,* vol. 2, no. 1, p. 36, 2021.

[40] Her, T.H., Finlay, R.J., Wu, C., Deliwala, S. and Mazur, E., , "Microstructuring of silicon with femtosecond laser pulses," *Applied Physics Letters,* vol. 73, no. 12, pp. 1673-1675, 1998.

[41] Vorobyev, A. Y., & Guo, C. , "Multifunctional surfaces produced by femtosecond laser pulses," *Journal of Applied Physics,* vol. 103, no. 2, p. 023108, 2008.

[42] Nolte, S., Will, M., Burghoff, J. and Tuennermann, A., , "Femtosecond waveguide writing: a new avenue to three-dimensional integrated optics," *Applied Physics A,* vol. 77, pp. 109-111, 2003.

[43] Zhang, Q., Yang, D., Qi, J., Cheng, Y., Gong, Q. and Li, Y.,, "Single scan femtosecond laser transverse writing of depressed cladding waveguides enabled by three-dimensional focal field engineering," *Optics Express,* vol. 12, no. 25, pp. 13263-13270, 2017.

[44] Gan Yuan, Yu Liu, Fei Xie,Chunlei Guo, Chi-Vinh Ngo, and Wei Li, "Fabrication of Superhydrophobic Gully-Structured Surfaces by Femtosecond Laser and Imprinting for High-Efficiency Self-Cleaning Rain Collection," *Langmuir,* vol. 38, pp. 2720-2728, 2022.

[45] Baldeweck, T., Balu, M., Batista, A., Vecker, W., Belousov, V.V., Breinig, H.G., Breymayer, J., Brizion, S., Castello, M., Chandra, D. and Choi, H., , "Multiphoton Microscopy and Fluorescence Lifetime Imaging: Applications in Biology and Medicine," *Walter de Gruyter GmbH & Co KG,* 2018.

[46] Palanker, D.V., Blumenkranz, M.S., Andersen, D., Wiltberger, M., Marcellino, G., Gooding, P., Angeley, D., Schuele, G., Woodley, B., Simoneau, M. and Friedman, N.J., , "Femtosecond laser–assisted cataract surgery with integrated optical coherence tomography," *Science translational medicine,* vol. 58, no. 2, pp. 58ra85-58ra85, 2010.

[47] Anderson, M., Ediger, A., Tsubaki, A., Zuhlke, C., Alexander, D., Gogos, G. and Shield, J.E., "Surface and microstructure investigation of picosecond versus femtosecond laser pulse processed copper," *Surface and Coatings Technology,* vol. 409, p. 126872, 2021.

[48] Zhang, W., Wen, X., Yang, S., Berta, Y. and Wang, Z.L., ", Berta, Y. and Wang, Z.L.Single-crystalline scroll-type nanotube arrays of copper hydroxide synthesized at room temperature," *Advanced materials, ,* vol. 15, no. 10, pp. 822-825, 2003.

[49] McHale, J.P., Garimella, S.V., "Bubble nucleation characteristics in pool boiling of a wetting liquid on smooth and rough surfaces," *Int. J. Multiph. Flow ,* vol. 36, no. 4, pp. 249-260, 2010.

[50] Berenson, P.J. , "Experiments on pool-boiling heat transfer," *Int. J. Heat Mass Transfer ,* vol. 10, no. 5, p. 985–999, 1962.

[51] Parker, J.L., El-Genk, M.S., "Enhanced saturation and subcooled boiling of FC-72 dielectric liquid, Int.," *Journal Heat Mass Transfer,* vol. 48, no. 18, p. 3736–3752, 2005.

[52] El-Genk, M.S., Parker, J.L. , "Enhanced boiling of HFE-7100 dielectric liquid on porous graphite," *Energy Convers. Manage,* vol. 15–16, no. 46, p. 2455–2481, 2005.

[53] Nishikawa, K., Ito, T., Tanaka, K. , "Enhanced heat transfer by nucleate boiling on a sintered metal layer.," *Heat Transfer – Jpn. Res. ,* vol. 8, no. 2, p. 65–81, 1979.

[54] Lu, S.M., Chang, R.H. , "Pool boiling from a surface with a porous layer," *AIChE Journal ,* vol. 33, no. 11, p. 1813–1828, 1987.

[55] Webb, R.L.,, "Nucleate boiling on porous coated surfaces," *Heat Transfer Eng.,* Vols. 3-4, no. 4, pp. 71-82, 1981.

[56] Chien, L. and Chang, C.C., "Experimental study of evaporation resistance on porous surfaces in flat heat pipes," in *Proceedings of 8th IEEE Intersociety Conference on Thermal and Thermomechanical Phenomena in Electronic Systems (ITherm)* , San Diego, CA, 2002.

[57] Chang, J.Y., You, S.M. , "Boiling heat transfer phenomena from microporous and porous surfaces in saturated FC-72," *Int. J. Heat Mass Transfer ,* vol. 40, no. 18, p. 4437–4447, 1997.

[58] Hsu,Y.Y. , "On the size range of active nucleation cavities on a heating surface," *Journal Heat Transfer ,* vol. 84, no. 3, p. 207, 1962.

[59] Ranjan, R., Murthy, J.Y., Garimella, S.V., "Bubble dynamics during capillary-fed nucleate boiling in porous media," in *Proceedings of 13th IEEE Intersociety Conference on Thermal and Thermomechanical Phenomena in Electronic Systems (ITherm), San Diego, CA.*, 2012.

[60] Igor Pioro; Warren M. Rohsenow; Doerffer, S. S. , "Nucleate Pool-boiling Heat Transfer - II. Assessment of Prediction Methods," *INTERNATIONAL JOURNAL OF HEAT AND MASS TRANSFER,* 2004.

[61] Samuel Siedel; Serge Cioulachtjian; Anthony J. Robinson; Jocelyn Bonjour, "Electric Field Effects During Nucleate Boiling from An Artificial Nucleation Site," *EXPERIMENTAL THERMAL AND FLUID SCIENCE,* 2011.

[62] Suchismita Sarangi; Justin A. Weibel; Suresh V. Garimella, "Effect of Particle Size on Surface-coating Enhancement of Pool Boiling Heat Transfer," *INTERNATIONAL JOURNAL OF HEAT AND MASS TRANSFER,* 2015.

[63] Jinsub Kim; Seongchul Jun; Ram Laksnarain; Seung M. You; , "Effect of Surface Roughness on Pool Boiling Heat Transfer at A Heated Surface Having Moderate Wettability," *INTERNATIONAL JOURNAL OF HEAT AND MASS TRANSFER,* 2016.

[64] Amir Mirza Gheitaghy; Hamid Saffari; Mokhtar Mohebbi; , "Investigation Pool Boiling Heat Transfer in U-shaped Mesochannel with Electrodeposited Porous Coating," *EXPERIMENTAL THERMAL AND FLUID SCIENCE,* 2016.

[65] Kai Wang; Nejdet Erkan; Haiguang Gong; Laishun Wang; Koji Okamoto, "Comparison of Pool Boiling CHF of A Polished Copper Block and Carbon Steel Block on A Declined Slope," *JOURNAL OF NUCLEAR SCIENCE AND TECHNOLOGY,* 2018.

[66] Biao Shen; Takeshi Hamazaki; Wei Ma; Naoki Iwata; Sumitomo Hidaka; Atsushi Takahara; Koji Takahashi; Yasuyuki Takata; , "Enhanced Pool Boiling of Ethanol on Wettability-patterned Surfaces," *APPLIED THERMAL ENGINEERING,* 2019.

[67] Jun, S., Kim, J., You, S.M., Kim, H.Y. , "Effect of heater orientation on pool boiling heat transfer from sintered copper microporous coating in saturated water,," *Int. J. Heat Mass Transf. ,* vol. 103, p. 277–284, 2016.

[68] Romashevskiy, S.A., Agranat, M.B. and Dmitriev, A.S., "Thermal training of functional surfaces fabricated with femtosecond laser pulses," *High Temperature,* vol. 54, pp. 461-465, 2016.